

Anelasticity and spherical-wave AVO-modelling in VTI-media

Arnim B. Haase and Charles P. Ursenbach

ABSTRACT

Anelasticity modifies VTI AVO responses. When reflection amplitude losses due to attenuation are compensated for by unit reflectivity scaling and spreading factor scaling, AVO-characteristics similar to the elastic situation are found. Q-factor dependence of spherical wave AVO is found to be strongest near critical angles. This Q-dependence, to some degree, mimics depth dependence of elastic comparisons.

INTRODUCTION

Taking spherical-wave AVO-modelling beyond isotropic situations acknowledges the fact that in many settings anisotropy is observed. In addition to anisotropy, matters are complicated by ever present anelastic effects. All rocks encountered in nature are anelastic to some degree. As was reviewed in previous work (Haase and Ursenbach, 2004), anelasticity causes attenuation and velocity dispersion of seismic waves. Frequency dependence of velocities because of dispersion can be quantified by frequency independent quality factors Q . Q-factor dependence of AVO has been observed in isotropic spherical-wave AVO-models and should also be expected for VTI-situations. In this contribution we seek to quantify the sensitivity of spherical-wave AVO-responses with respect to finite Q-factors of VTI-media.

THEORY

The same mathematical treatment of anelasticity found in Aki and Richards (1980) and used in previous work (Haase and Ursenbach, 2004) also applies to anisotropic situations. Aki and Richards show that causality requires velocity dispersion and derive the following equation:

$$v(\omega) = v_{ref} \left(1 + \frac{\ln\left(\frac{\omega}{\omega_{ref}}\right)}{\pi Q} - \frac{i}{2Q} \right) \quad (1)$$

where Q is a frequency independent quality factor. Therefore, for anelastic models, velocities are complex and must be recomputed for every frequency point, according to equation (1).

The equations for modelling an explosive source (point source) are shown in Haase and Ursenbach (2005) and repeated here:

$$S_r = \frac{iB\omega^2}{4\pi c_{33}c_{55}} \int_0^\infty R_{PP}(p_0) J_1(\omega p_0 r) e^{-i\omega\xi(z+h)} \times \frac{p_0^2 [c_{55}p_0^2 + (c_{33} - [c_{13} + c_{55}])\xi^2 - \rho]}{\xi(\xi^2 - \eta^2)} dp_0 \quad (2)$$

$$S_\phi = 0$$

$$S_z = -\frac{B\omega^2}{4\pi c_{33}c_{55}} \int_0^\infty R_{PP}(p_0) J_0(\omega p_0 r) e^{-i\omega\xi(z+h)} \times \frac{p_0 [(c_{11} - [c_{13} + c_{55}])p_0^2 + c_{55}\xi^2 - \rho]}{(\xi^2 - \eta^2)} dp_0 \quad (3)$$

where $R_{PP}(p_0)$ and the vertical slownesses ξ and η are given from plane-wave analysis (Graebner, 1992; Rueger, 1996). Similar equations have been developed for the converted wave case. The mathematical details can be found in Ursenbach and Haase (2005).

The integrations shown in equations (2) and (3) compute particle motion, one frequency point at a time. Then we proceed as in the isotropic situation: When all frequency points have been computed for the desired output bandwidth, the time domain response is found by inverse Fourier transform, and quadrature traces are determined by Hilbert transform; from these two trace types spherical-wave amplitudes are calculated.

MODELLING

The two-layer model that was utilized in the isotropic AVO study (Haase, 2004) is also employed here: The layer parameters are $\alpha_1 = 2000$ m/s, $\beta_1 = 879.88$ m/s, $\rho_1 = 2400$ kg/m³, $\alpha_2 = 2933.33$ m/s, $\beta_2 = 1882.29$ m/s and $\rho_2 = 2000$ kg/m³. As before, a 5/15-80\100 Ormsby wavelet is chosen as the source signature; a P-wave point source is assumed. VTI-type anisotropy of the top layer is introduced in two steps: weak anisotropy ($\varepsilon = 0.15$, $\delta = 0.05$) and moderate anisotropy ($\varepsilon = 0.3$, $\delta = 0.1$); the bottom layer is always assumed to be isotropic. VTI radiation patterns and free surface effects are again ignored.

All layer velocities given above are considered to be 50 Hz reference velocities for the anelastic situation. Two values are assumed for the top layer P-wave quality factor: firstly, $Q_{P1} = 100$ and secondly, $Q_{P1} = 387.5$. The other Q-factors are calculated from α , β , and Q_{P1} utilizing empirical equations given by Waters (1978) and Udias (1999) and listed in Tables 1 and 2:

$$1/Q_P = \left(\frac{const.}{\alpha} \right)^2 \quad (4)$$

$$Q_S = Q_P \frac{4}{3} \left(\frac{\beta}{\alpha} \right)^2 \quad (5)$$

Table 1. Q-factors derived from $Q_{P1}=100$.

Class	Q_{P1}	Q_{P2}	Q_{S1}	Q_{S2}
1	100	215.1	25.8	118.1

Table 2. Q-factors derived from $Q_{P1}=387.5$.

Class	Q_{P1}	Q_{P2}	Q_{S1}	Q_{S2}
1	387.5	833.5	100	457.6

All Q-factors are considered to be isotropic in this study.

As explained in Haase and Ursenbach (2005), the appearance of the computed AVO results depends on scaling and spherical spreading must be compensated for if results are to be compared to plane-wave responses. The P-wave examples shown in this report give magnitude displays normalized to the response magnitude obtained when reflection coefficients R_{PP} in equations (2) and (3) are set to unity. When R_{PS} is set to unity for C-wave examples, the scaling at small incidence angles is oscillatory. In this region geometrical spreading factors are computed (Krebes and Slawinski, 1991) and calibrated to plane wave responses. These calibrated geometrical spreading factors depart from unity R_{PS} scaling at large incidence angles. For the converted wave case the Figures shown give magnitude displays scaled by a combination of unity R_{PS} and calibrated geometrical spreading factors with a transition region at the midrange of incidence angles. Figure 1 of Haase and Ursenbach (2005) gives an example for this mode of scaling.

Figures 1 and 3 show the Q-dependence of AVO Class I spherical C-wave responses for weak and moderate VTI at $z = 500$ m. Figures 2 and 4 display the equivalent P-wave responses. Figures 5 and 6 demonstrate depth dependence of weak VTI spherical wave AVO for $Q = 387$. The dependence of spherical wave AVO on VTI strength for $Q = 387$ at $z = 500$ m can be seen in Figures 7 and 8. In computing these figures, actual particle motion is projected onto the ray direction for P-waves and onto the perpendicular to the ray direction for C-waves.

DISCUSSION AND CONCLUSIONS

The Class I AVO model used here has a velocity increase across the interface. Increasing top layer VTI-type anisotropy decreases this velocity contrast and a shift of the critical point towards larger angles is found in the elastic situation (Haase and Ursenbach, 2005). Figures 7 and 8 find the same result for the anelastic case. Spherical wave VTI AVO depth dependence is displayed in Figures 5 and 6. Larger depths “tweak” the AVO response near the critical point to lower angles toward a plane wave comparison. Similarly, VTI AVO responses are also “tweaked” by a change in Q-factors.

Figures 1 and 2 (weak VTI) as well as Figures 3 and 4 (moderate VTI) show a shift away from plane wave comparisons with decreasing Q-factors. In other words, increasing Q-factors and increasing depths move normalized spherical wave AVO closer to plane wave comparisons, as was observed in the isotropic situation. Both C-wave AVO and P-wave AVO are more sensitive to changes in anisotropy than to changes in depth or Q-factors. In addition, spherical C-waves are more sensitive to increasing attenuation than spherical P-waves in these examples.

In anisotropic materials particle motion is not in the propagation direction for P-waves or perpendicular to the propagation direction for S-waves. The terms used in the literature are quasi-P-waves (qP) and quasi-S-waves (qS). For the above displays the actual particle motion is projected onto the propagation direction (at the ray angle) for P-waves and onto the ray angle perpendicular for C-waves.

REFERENCES

- Aki, K.T., and Richards, P.G., 1980, Quantitative Seismology: Theory and Methods: Vol. 1, W.H. Freeman and Co.
- Graebner, M., 1992, Plane-wave reflection and transmission coefficients for a transversely isotropic solid: *Geophysics*, **57**, 1512-1519.
- Haase, A.B., 2004, Spherical wave AVO modeling of converted waves in isotropic media: 74th Ann. Internat. Mtg. Soc. Expl. Geophys, 263-266.
- Haase, A.B., and Ursenbach, C.P., 2004, Anelasticity and spherical wave AVO-modelling in isotropic media: CREWES Research Report, Volume **16**.
- Haase, A.B., and Ursenbach, C.P., 2005, Spherical-wave AVO-modelling in elastic VTI-media: CREWES Research Report, **17**.
- Krebes, E.S., and Slawinski, M.A., 1991, On raytracing in an elastic-anelastic medium: *Bulletin of the Seismological Society of America*, **81**, 667-686.
- Rueger, A., 1996, Reflection coefficients and azimuthal AVO analysis in anisotropic media: Ph.D. Thesis, Colorado School of Mines.
- Udias, A., 1999, Principles of seismology: Cambridge University Press, page 260.
- Ursenbach, C.P., and Haase, A.B., 2005, Derivation of generalized reflections from point sources in a two-layer VTI medium: CREWES Research Report, **17**.
- Waters, K.H., 1978, Reflection Seismology: John Wiley and Sons, Inc., page 203.

ACKNOWLEDGEMENTS

The authors wish to thank Professor E. Krebes for his help with the theory. Support by the CREWES team and its industrial sponsorship is gratefully acknowledged.

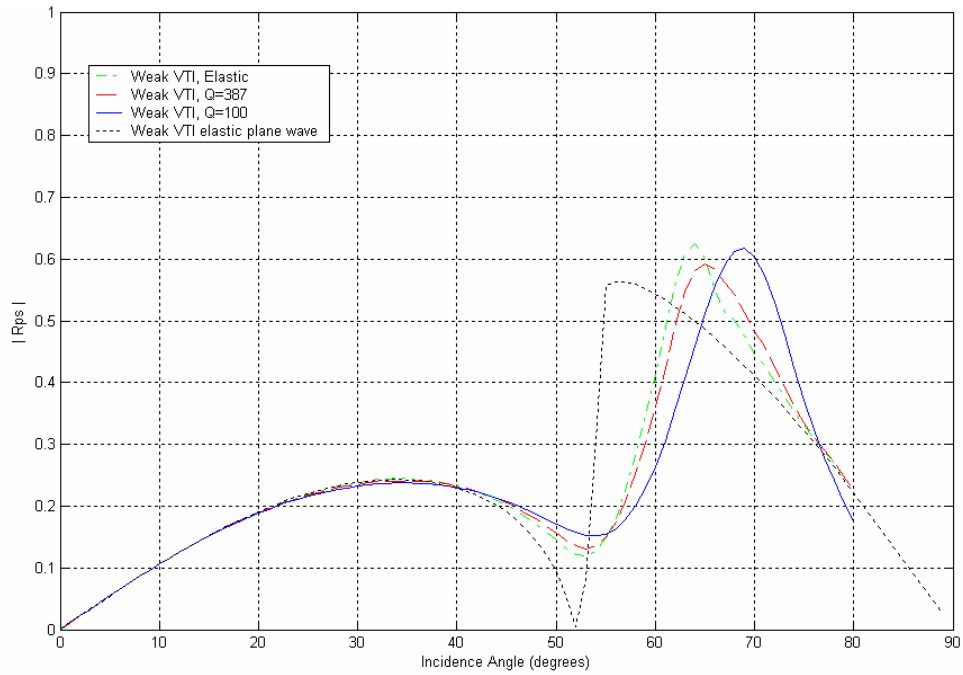


FIG. 1. Weak VTI AVO-Class 1 spherical wave PS reflection coefficient (z=500m).

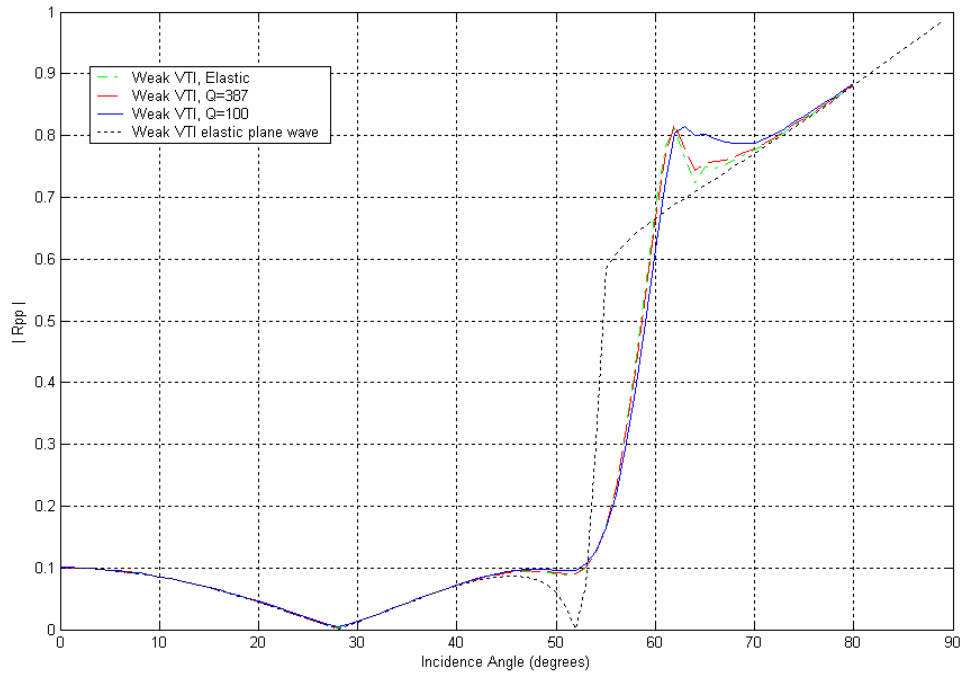


FIG. 2. Weak VTI AVO-Class 1 spherical wave PP reflection coefficient (z=500m).

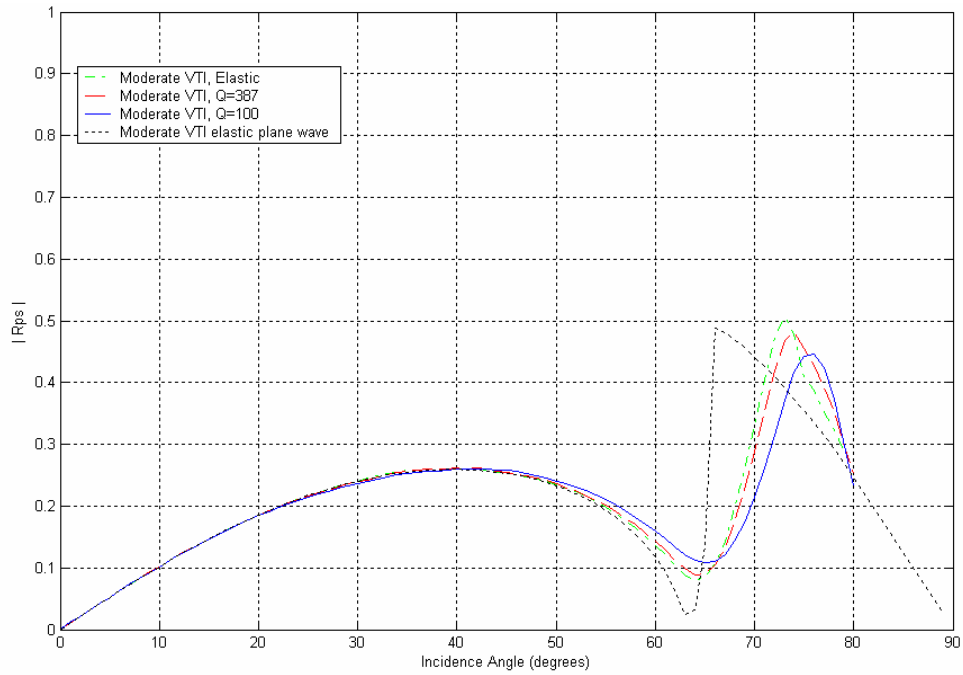


FIG. 3. Moderate VTI AVO-Class 1 spherical wave PS reflection coefficient ($z=500\text{m}$).

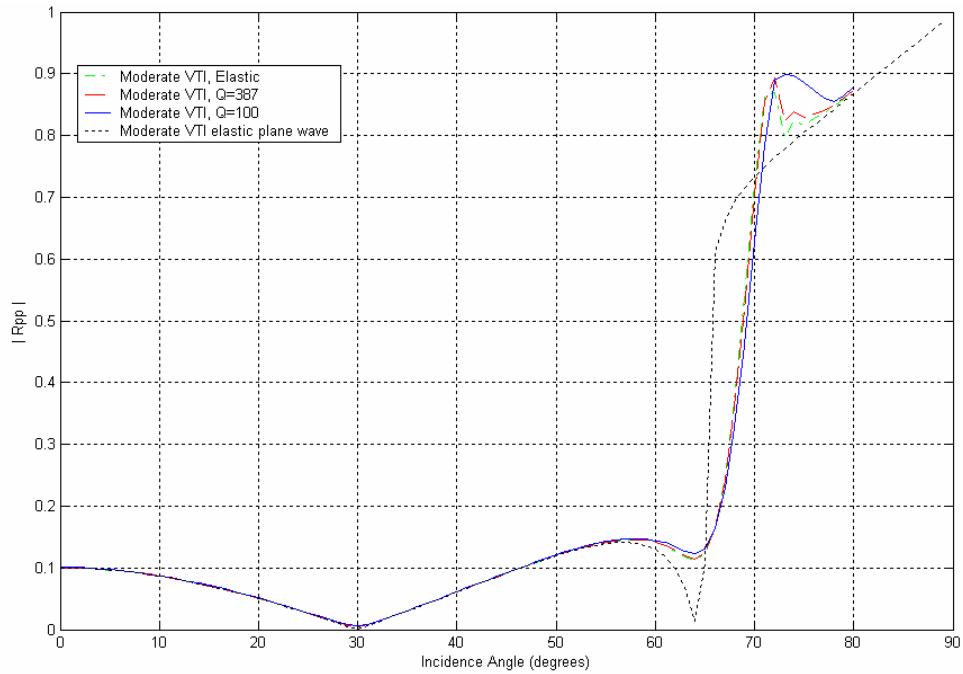


FIG. 4. Moderate VTI AVO-Class 1 spherical wave PP reflection coefficient ($z=500\text{m}$).

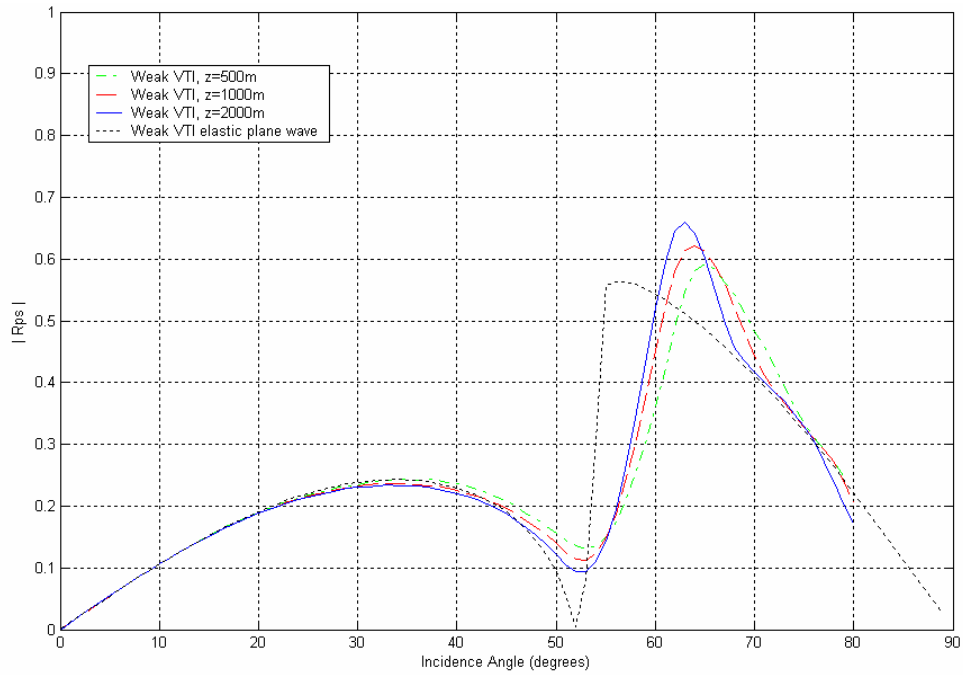


FIG. 5. Weak VTI AVO-Class 1 spherical wave PS reflection coefficient (Q=387).

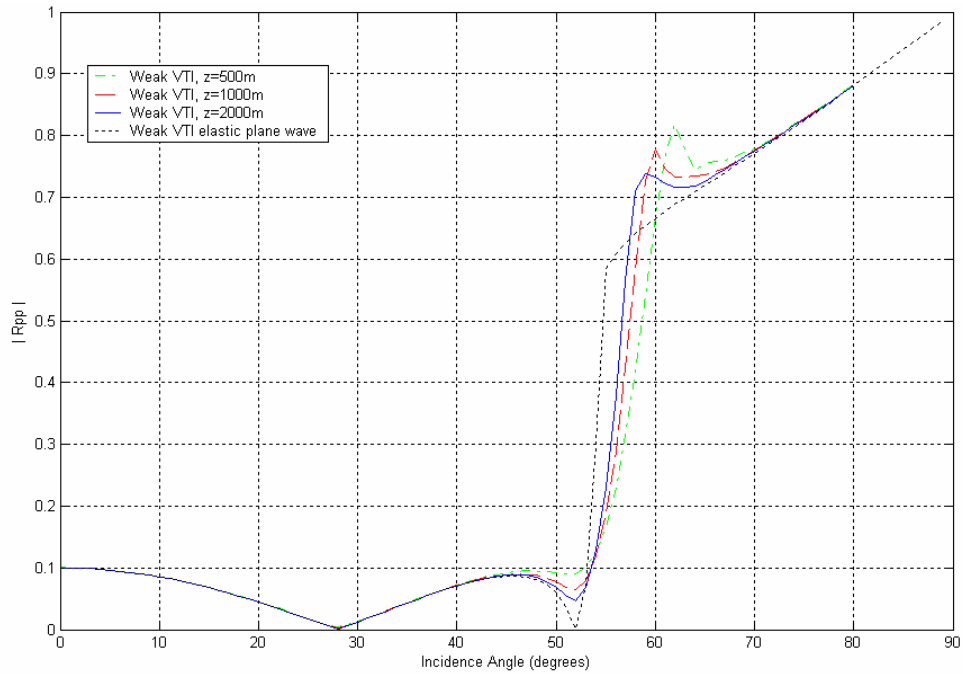


FIG. 6. Weak VTI AVO-Class 1 spherical wave PP reflection coefficient (Q=387).

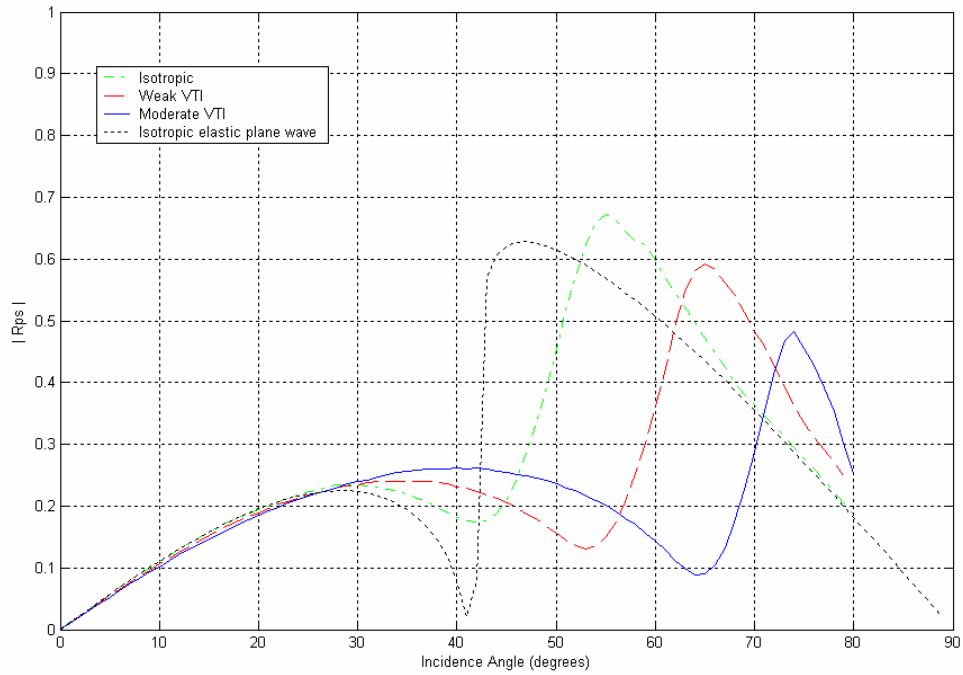


FIG. 7. VTI AVO-Class 1 spherical wave PS reflection coefficient ($Q=387, z=500m$).

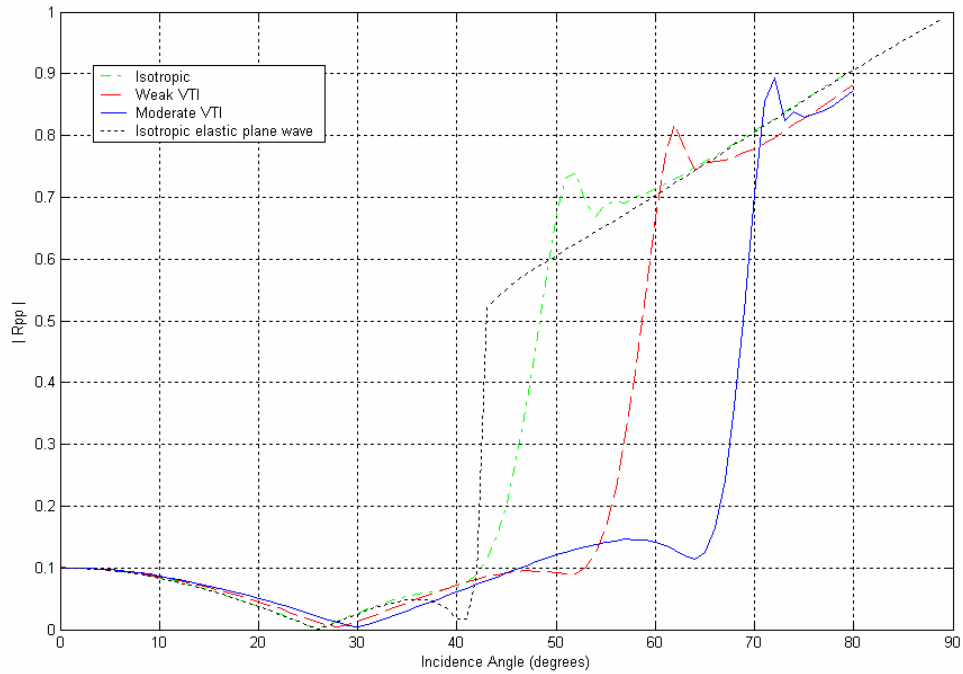


FIG. 8. VTI AVO-Class 1 spherical wave PP reflection coefficient ($Q=387, z=500m$).